Petroleum Science 19 (2022) 2895–2904

Contents lists available at ScienceDirect

Petroleum Science

journal homepage: www.keaipublishing.com/en/journals/petroleum-science

Original Paper

Impact of flow rate on dynamic imbibition in fractured tight sandstone cores

Yi-Fei Liu [a, b], Cai-Li Dai [a, b, *], Chen-Wei Zou [a, b], Qing You [c, **], Ming-Wei Zhao [a, b], Guang Zhao [a, b], Yong-Peng Sun [a, b]

[a] Shandong Key Laboratory of Oilfield Chemistry (China University of Petroleum (East China)), Qingdao, 266580, Shandong, China
[b] Key Laboratory of Unconventional Oil & Gas Development (China University of Petroleum (East China)), Ministry of Education, Qingdao, 266580, Shandong, China
[c] School of Energy Resources, China University of Geosciences, Beijing, 100083, China

ARTICLE INFO

Article history:
Received 2 May 2022
Received in revised form
19 July 2022
Accepted 26 July 2022
Available online 31 July 2022

Edited by Yan-Hua Sun

Keywords:
Tight oil
Dynamic imbibition
Flow rate
Oil recovery
Nuclear magnetic resonance

ABSTRACT

Dynamic imbibition, which is significantly affected by flow rate, plays an important role in the development of tight oil. This study investigated the impact of flow rate on dynamic imbibition in fractured tight sandstone cores via online nuclear magnetic resonance core-flooding experiments. The oil expulsion efficiency and capillary number of multiscale pores were quantitatively analyzed to elucidate the influence of flow rate on the oil recovery during dynamic imbibition. The pores of the cores used were divided into micropores (0.01–1.00 μm in diameter), mesopores (1.00–30.00 μm in diameter), and macropores (30.00–400.00 μm in diameter) by matching the T_2 spectrum and the mercury intrusion data. The volume proportion of micropores was 52.0%, and that of macropores was 19.0%. The total oil recovery of the core was found to reach 29.8% at the optimal flow rate of 0.1 mL/min. At the optimal flow rate, the oil recovery of micropores reached 50.4%, followed by that of macropores (28.6%), and that of mesopores was the lowest (15.8%). The oil expulsion efficiency, the capillary number, and the contribution to total oil recovery of micropores significantly increased with the decrease in flow rate, while those of macropores decreased. This was caused by the synergy of capillary force and displacement pressure. During dynamic imbibition at a low flow rate, the oil in micropores was effectively expelled driven by capillary force, and the effect of displacement pressure was weak, leading to large amounts of remaining oil trapped in macropores. On the contrary, when the flow rate was too high, large amounts of remaining oil would be trapped in micropores. Only at a moderate flow rate did the capillary force and displacement pressure both have significant effects on oil expulsion, and the oil in different sized pores was effectively expelled, thus generating a relatively high total oil recovery.

1. Introduction

The demand for oil consumption has been increasing with the development of society and the economy. The scale of tight oil resources has reached 2–3 times more than that of conventional oil and gas resources (Zou et al., 2012, 2015). The efficient development of tight oil is crucial to ensuring the energy supply. In recent years, it has gradually become a focused area of global attention (Li et al., 2017). Tight reservoirs have a small pore scale, a high water injection pressure, and limited development methods. The high flow resistance in tight sandstone results in the low natural productivity of tight reservoirs (Meng et al., 2018). Hydraulic fracturing is thus a necessary means for the development of tight oil reservoirs, in which different grades of natural fractures are usually developed (Sun et al., 2019; Zhu et al., 2019). Hydraulic fracturing can generate artificial fractures to connect natural fractures to form a fracture system, thereby allowing the crude oil in the matrix to flow to the fracture system and then be output from the oil well. However, the tight sandstone matrix is characterized by low permeability (usually less than 1 mD) and a small pore size (usually on the nanometer or micrometer scale), making it difficult to displace the crude oil from the matrix to the fractures via conventional water flooding (Meng et al., 2018). Due to the small pore

* Corresponding author. Shandong Key Laboratory of Oilfield Chemistry (China University of Petroleum (East China)), Qingdao, 266580, Shandong, China.
** Corresponding author. School of Energy Resources, China University of Geosciences, Beijing, 100083, China.
E-mail addresses: daicl@upc.edu.cn (C.-L. Dai), youqing@cugb.edu.cn (Q. You).

https://doi.org/10.1016/j.petsci.2022.07.007

diameter, the capillary force plays a significant role, and the imbibition effect relying on the capillary force is significant for the production of the matrix crude oil (Morrow and Mason, 2001).

Imbibition refers to the phenomenon in which the wetting-phase liquid displaces the non-wetting-phase liquid via capillary force during two-phase fluid displacement in porous media, which has become an important replacement method for tight oil development. Imbibition can be divided into static and dynamic imbibition (Dou et al., 2021). Static imbibition refers to the situation in which the extra-matrix fluid is in a static state. This process occurs without external differential pressure, which is mainly affected by the capillary force. Scholars have conducted extensive experimental and theoretical research on the influence of static imbibition, and have established scaling imbibition models (Al-Attar, 2010; Babadagli, 2002; Civan and Rasmussen, 2003, 2005; Hatiboglu and Babadagli, 2007; Meng et al., 2016; Tavassoli et al., 2005; Wang et al., 2019; Yang et al., 2016; Yildiz et al., 2006). The main influencing factors of static imbibition are the matrix permeability, porosity, surface tension, wettability, boundary conditions, fracture density, crude oil viscosity, and water saturation. In addition, the imbibition recovery rate of tight sandstone is very low without the addition of surfactants. Surfactants have an excellent ability to reduce the oil–water interfacial tension and change the wettability of the rock surface, which can reduce the adhesion of the crude oil on the surface of the matrix pores and increase the capillary force, thereby significantly improving the imbibition recovery rate (Adibhatla and Mohanty, 2008; Fallah Fini et al., 2012; Kathel and Mohanty, 2013; Meng et al., 2018; Sharma and Mohanty, 2013; Sun et al., 2020; Wang et al., 2017; You et al., 2018).

However, during oil recovery, the fluids flow in the fractures and the matrices, where additional displacement pressure complicates the imbibition process (Wang et al., 2017). In contrast to static imbibition, this is called dynamic imbibition. Previous studies have explored the effects of wettability, oil–water interfacial tension, fluid viscosity ratio, displacement pressure difference, flow rate, and other factors on the recovery factor of dynamic imbibition (Dai et al., 2019; Dou et al., 2021; Sun et al., 2020; Tangirala and Sheng, 2019; Wang et al., 2017, 2018; Yang et al., 2019). Previous research has shown that the displacement flow rate has a substantial influence on the dynamic imbibition recovery factor (Dai et al., 2019; Dou et al., 2021; Sun et al., 2020). However, limited by the experimental research methods, the oil–water distribution characteristics, the evolution laws, and the influence mechanisms in pores of different scales during the dynamic imbibition process remain unclear, which is not conducive to the understanding and optimization of the dynamic imbibition process.

There are generally two methods used for imbibition experiments, namely traditional core simulation and nuclear magnetic resonance (NMR). Traditional core simulation experiments, on which most previous studies were based, are based on mass or volume measurements (Al-Attar, 2010; Babadagli, 2002; Hatiboglu and Babadagli, 2007; Meng et al., 2018; Tangirala and Sheng, 2019; You et al., 2018). Although this method can reveal the influences of different parameters on the imbibition effect, it cannot be used to observe the internal structure of the core and the distribution of the oil and water in the porous medium during the imbibition process. Additionally, because the size of the tight sandstone core and the crude oil mass or volume used for the experiment are very small, the error of the experiment is undoubtedly increased. In recent years, advanced NMR technology has been used to quantitatively measure the hydrogen content in the pore fluids to characterize the internal structure of the tight sandstone, the oil or water content in pores of different sizes, and the evolution process (Cheng et al., 2018, 2019; Jiang et al., 2018; Liu and Sheng, 2020; Umeobi et al., 2021; Wang et al., 2018; Yang et al., 2019).

The present study investigates the influence of the flow velocity on dynamic imbibition. Via the use of online NMR core displacement technology, the influences of the flow rate on the overall oil recovery of the tight sandstone core and on the oil expulsion in pores of different sizes were systematically investigated. Via the calculation of the capillary number and the recovery factor ratio of pores of different sizes, the mechanism of the influence of the flow rate on the dynamic imbibition recovery is revealed. This study contributes to the understanding and optimization of the dynamic imbibition process.

2. Experimental

2.1. Materials

The water used was simulated formation brine, the components of which are listed in Table 1. The oil used was simulated oil prepared from dehydrated crude oil (Jimsar Block, Zhundong Oilfield, China) and kerosene at a volume ratio of 1:4. The simulated oil had a density of 0.82 g/cm^3 and a viscosity of 1.59 mPa s at 80 °C. The surfactant used in the experiment was amide sulfobetaine (ASB, Connaught Industry, Shanghai, China), and the ASB solution was prepared with simulated brine.

Core samples of the tight sandstone outcrop were collected from the upper Shaxi Temple Formation of the Middle Jurassic in Sichuan, China. The physical parameters of the core samples are reported in Table 2.

2.2. Methods

2.2.1. Static imbibition experiment

The static imbibition device is shown in Fig. 1. The device was composed of an imbibition bottle, a graduated glass tube (accuracy ±0.01 mL), and a silastic tube. After the core was placed in the imbibition bottle, the imbibition agent was added through the silastic tube.

The experimental process is as follows.

(1) The core was cut, cleaned, and dried at 110 °C for more than 48 h, and the dry weight m_0 of the core was recorded.
(2) The core was saturated with oil by vacuuming and pressurization. After the oil was saturated, the core was placed in the oil in a constant-temperature water bath at 80 °C for 24 h to avoid the influence of thermal expansion on the saturated oil content in the core pores.
(3) The core was then removed, the surface of the core was wiped with oil-absorbing paper, the mass m_1 of the core saturated with oil was recorded, and the saturated oil amount was calculated.
(4) The core was placed in an imbibition bottle, which was then sealed with vaseline, and the surfactant solution was then slowly injected into the imbibition bottle through a rubber tube at a constant temperature of 80 °C until the core was completely covered and the graduated glass tube was filled.
(5) After the rubber tube was sealed with a clip, the imbibition bottle was placed in a constant-temperature water bath at 80 °C, the upper and lower scales of the oil phase in the graduated glass tube were read at regular intervals, and the imbibition oil volume V_o and recovery factor E_R were calculated, as given by Eq. (1).

$$E_R = \frac{V_o \times \rho_o}{m_1 - m_0} \times 100\%, \quad (1)$$

where E_R is the core imbibition recovery factor, %; V_o is the oil phase

Table 1
Ion concentration and salinity of the formation brine.

Ion concentration, mg/L							Total salinity, mg/L
Na^+	K^+	Ca^{2+}	Mg^{2+}	Cl^-	CO_3^{2-}	HCO_3^-	
9054.0	522.0	26.1	12.2	5880.0	271.1	14174.2	29776.2

Table 2
Key parameters of the core samples.

Sample No.	Porosity, %	Permeability, μm²	Diameter, mm	Length, mm
S-1	14.7	0.32	25.12	31.17
S-2	14.7	0.32	25.12	30.64
S-3	14.7	0.32	25.12	31.24
S-4	15.4	0.35	25.11	31.05
S-5	15.4	0.35	25.11	30.66
S-6	15.4	0.35	25.11	30.43
S-7	15.3	0.31	25.13	31.58
D-1	15.5	0.33	25.02	100.24
D-2	15.3	0.30	25.05	100.16
D-3	14.8	0.32	25.11	100.11
D-4	15.2	0.34	25.08	100.17
D-5	15.3	0.31	25.06	100.20
P-1	15.1	0.30	25.03	50.02
P-2	15.1	0.30	25.03	50.11

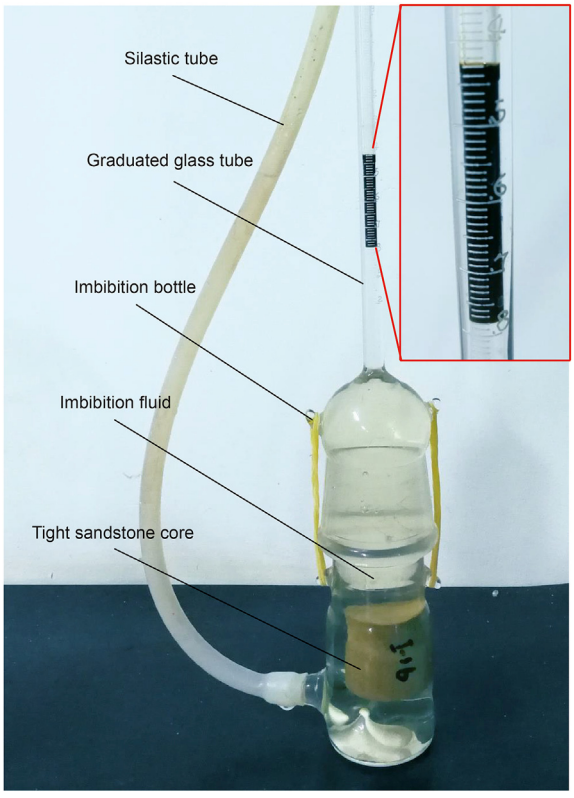

Fig. 1. The static imbibition device.

volume, mL; and ρ_o is the simulated oil density, $\rho_0 = 0.82$ g/cm^3.

2.2.2. Interfacial tension and contact angle measurements

The oil–water interfacial tension between the surfactant solution and simulated oil was measured using a rotating drop interfacial tensiometer (TX500C, CNG company, USA) at 80 °C. The simulated formation brine was used to prepare the surfactant solutions with different concentrations. The oil–water interfacial tension was calculated according to the equation provided in the work of You et al. (2018).

The contact angle between the surfactant solution/oil droplet/core were determined using a contact angle measuring instrument (JC2000D1, Shanghai Zhongchen Digital Technic Apparatus Co., Ltd, China) at 80 °C. The detailed experimental procedures and schematics are provided in the work of Liu et al. (2019).

2.2.3. Online NMR dynamic imbibition experiment

The oil expulsion and evolution in pores of different sizes were studied by an online NMR core displacement system (as shown in Fig. 2). The system was composed of an MacroMR low-field NMR detector (Suzhou Niumei Analytical Instrument Co., Ltd, China), a nuclear magnetic analysis system (Suzhou Niumei Analytical Instrument Co., Ltd, China), and a core displacement system. The magnet was a permanent magnet with a magnetic field strength of 0.3±0.05 T. The main frequency of the instrument was 12.8 MHz, and the diameter of the probe coil was 150 mm. The core displacement system consisted of an ISCO pump, a constant-temperature oil bath, a circulating pump, an intermediate vessel, a core holder, and a pressure sensor. The core holder was made of a non-magnetic material to eliminate the noise signal of the experimental device. The fluid used for confining pressure and temperature control was fluorine oil.

The experimental temperature was 80 °C, and the simulated water was prepared with heavy water to shield the hydrogen signal of the water phase. The tight sandstone outcrop core was cut into four symmetrical pieces along the lateral and vertical directions. Stainless steel sheets (0.5 mm) were sandwiched at the edges of both sides of the fracture along the length direction to fix the width of the main fracture. After the combination, it was placed in a core holder to simulate the tight oil matrix–fracture dual-medium flow unit.

The experimental process is as follows.

(1) The surfactant solution prepared with sufficient heavy water was added to an intermediate container, and the online NMR core displacement system was connected according to Fig. 2.
(2) The core was cut and cleaned according to the design, it was dried at 110 °C for more than 48 h, and the core was then saturated with oil via vacuuming and pressurization.
(3) Epoxy resin glue was applied to seal both ends of the core, and the cylindrical surface was sealed by the confining pressure. This way, the exchange of oil and water would only occur in the matrix near the fractures, and the influence of boundary conditions was eliminated.
(4) The temperature of the gripper containing the rubber sleeve was kept constant at 80 °C, and the T_2 signal was measured as the base signal.
(5) The combined core was placed in the holder and kept stable at 80 °C for 2 h. The T_2 signal at this time was measured as the initial T_2 spectrum of the matrix-fracture tight sandstone core.
(6) The confining pressure of the gripper was maintained at about 4.0 MPa, a constant temperature of 80 °C was set, and the surfactant solution was injected at a specific rate to carry out the dynamic imbibition process.

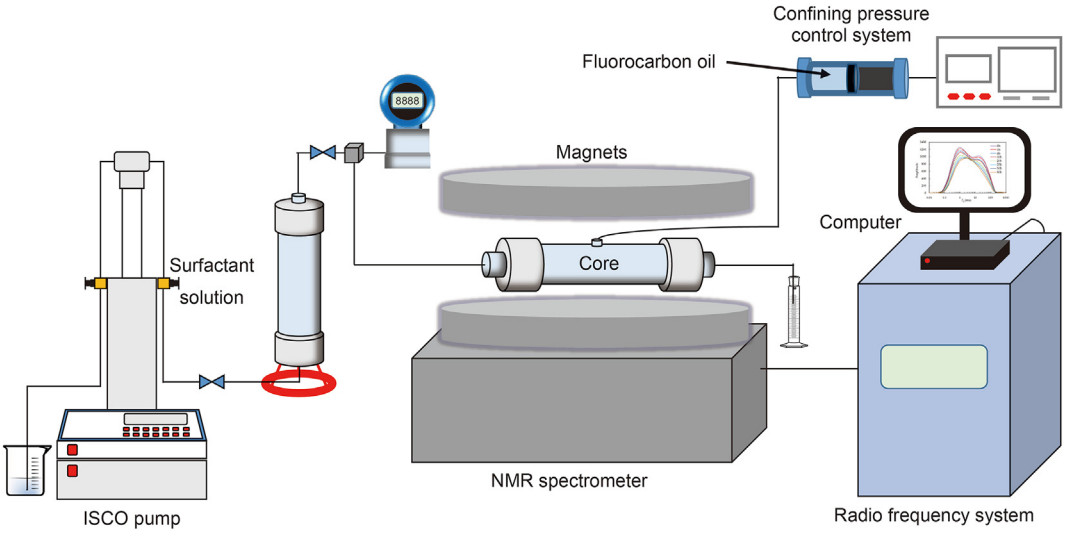

Fig. 2. The schematic diagram of the online NMR core displacement system.

(7) The matrix-fracture tight sandstone core was scanned at a specific time to obtain T_2 signals at different times until they were basically stable, which was regarded as the end of the dynamic imbibition process.
(8) The base signal was subtracted from all T_2 data to obtain T_2 spectra at different times, and the mercury intrusion data were matched to obtain the degree of oil phase production of different pores, as given by Eq. (2) (Cheng et al., 2018; Dai et al., 2019).

$$R = \frac{A_0 - A_t}{A_0} \times 100\%, \quad (2)$$

where R is the oil recovery factor, %; A_0 is the initial signal amplitude; and A_t is the signal amplitude at a certain time.

3. Results and discussion

3.1. Static imbibition effect

Different concentrations of ASB surfactant solutions were prepared using the simulated brine. The static imbibition effects using surfactant solutions with different concentrations were studied, and the changes of oil–water interfacial tension and rock surface wettability were measured to explore the reasons for the change of static imbibition recovery. The results of the ultimate oil recovery of static imbibition, the oil–water interfacial tension, and the contact angle between liquid/oil droplet/core surface are presented in Fig. 3.

With the increase in the concentration of the ASB surfactant, the final oil recovery of static imbibition was found to first increase and then decrease. The ultimate oil recovery reached the highest value of about 23.2% when the surfactant concentration was about 0.15%. This is because the amount of surfactant molecules adsorbed on the surface of pores and the oil–water interface changed with the increase in the surfactant concentration, which in turn changed the pore surface wettability and the oil–water interfacial tension. As shown in Fig. 3, the initial contact angle of oil droplet on the core surface was 26.6°, indicating the core surface was lipophilic. With the increase in surfactant concentration in brine, the contact angle of oil droplet on the core surface gradually increased. When the surfactant concentration was about 0.15%, the contact angle was the largest (135.2°), indicating that the core surface was reversed from

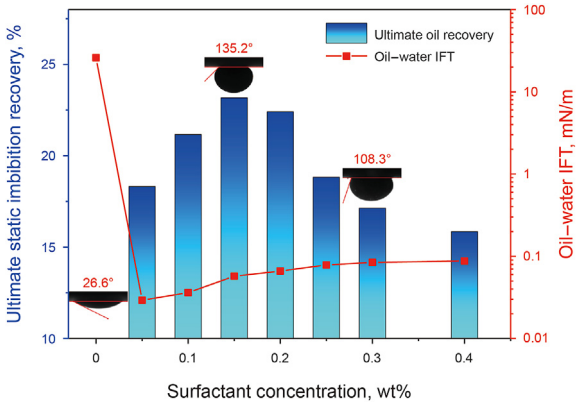

Fig. 3. Changes of the oil recovery, oil–water interfacial tension and contact angle with surfactant concentration.

lipophilic to hydrophilic, which was conducive to oil drainage by imbibition. In addition, with the increase in the surfactant concentration, the oil–water interfacial tension first decreased and then slightly increased. The interfacial tension reached the lowest value of about 2.9×10^{-2} mN/m when the surfactant concentration was 0.05%. Although the effect in reducing the interfacial tension was not optimal at the concentration of 0.15%, the interfacial tension value did not increase much as compared to that at the lowest value, and was still on the order of 10^{-2} mN/m. Based on the above discussion, it can be seen when the surfactant concentration was 0.15%, the pore surface wettability and the oil–water interfacial tension value reached the optimal range. Thus, the difference between the capillary force (oil displacement power) and the adhesion work (oil displacement resistance) reached the maximum, and the static imbibition achieved the highest ultimate oil recovery. Therefore, considering the properties of static imbibition and the ability to reduce the interfacial tension of different concentrations of the ASB surfactant, the optimized ASB concentration for the subsequent dynamic imbibition experiments was 0.15%.

3.2. Effect of the flow rate on the oil recovery of core during dynamic imbibition

The sum of amplitudes in T_2 spectrum is defined as the total oil

phase signal, which represents the oil amount in the core. According to the variation of total oil phase signal at different moments during dynamic imbibition process of the matrix-fracture tight sandstone core, the oil recovery of the core during the dynamic imbibition process could be calculated by Eq. (2). Fig. 4a presents the typical T_2 spectra during the dynamic imbibition process with a displacement flow rate of 0.1 mL/min. It can be seen that with the progression of dynamic imbibition, the amplitudes in T_2 spectra gradually decreased, which means the oil was continuously expelled from the core, indicating an increase in oil recovery. Fig. 4b exhibits the variation in the total oil phase signal and the corresponding oil recovery during the dynamic imbibition calculated based on Fig. 4a. With the progress in dynamic imbibition process, the total oil phase signal gradually decreased because of the continuous oil expulsion, and the corresponding oil recovery gradually increased to about 30%.

Furthermore, with the assistance of online NMR, the T_2 spectra of the series of dynamic imbibition experiments under different displacement flow rates were obtained. Via the method described previously, the dynamic imbibition recovery factors of the tight sandstone matrix-fracture cores under different displacement flow rates were calculated. The core samples numbered D-1 to D-5 were used for the dynamic imbibition NMR tests using a 0.15% ASB surfactant solution prepared in the heavy water, and the injection rate gradients were set as 0.4, 0.2, 0.1, 0.05, and 0.02 mL/min. Fig. 5 exhibits the results of the ultimate dynamic imbibition recovery of the tight sandstone cores under different displacement flow rates.

As shown in Fig. 5, with the decrease in the displacement flow rate, the dynamic imbibition oil recovery first increased obviously and then decreased. When the displacement flow rate was moderate (about 0.1 mL/min), the dynamic imbibition oil recovery reached the maximum, and increased from 15.1% (under the high flow rate of 0.4 mL/min) to 29.8%. Therefore, the flow velocity in the fracture should be controlled to achieve the best dynamic imbibition oil recovery; a too-low or too-high displacement flow velocity is not conducive to the optimal total recovery.

To determine the reasons for these results, it was necessary to study the effect of the displacement flow rate on the oil expulsion characteristics of different-sized pores. Therefore, the subsequent experiments relied on the NMR T_2 spectrum to divide the pore scale, and the influence of the displacement flow rate of the dynamic imbibition process on the oil expulsion efficiency in pores of different scales was investigated.

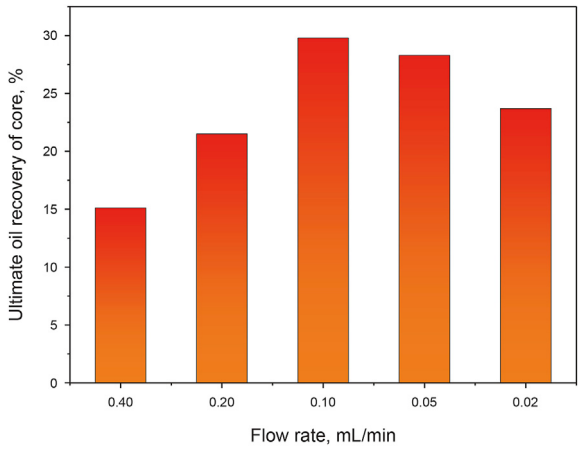

Fig. 5. The effect of the displacement flow rate on the dynamic imbibition recovery factor.

3.3. Oil expulsion in pores of different sizes

To quantitatively analyze the oil expulsion characteristics of pores of different sizes, it was necessary to divide the pores into different scales. By matching the T_2 spectrum and the mercury intrusion data, the range of pores of different scales was divided. The oil recovery factors of the pores of different scales were then calculated according to Eq. (2) via the change in the amplitude of the spectral curve.

The conversion relationship between the relaxation time T_2 and the pore diameter when the pores are saturated with the oil phase is given by Eq. (3) (Lowden et al., 1998).

$$d = CT_2, \tag{3}$$

where T_2 is the relaxation time, ms; C is the conversion coefficient, μm/ms; and d is the pore diameter, μm.

A tight sandstone core was cut into two cylindrical cores (numbered P-1 and P-2). Core sample P-1 was used for the mercury intrusion test, and core sample P-2 was saturated with oil for the NMR test. The obtained T_2 spectrum was matched with the mercury intrusion data, as shown in Fig. 6. To calculate the conversion coefficient between the pore diameter and the relaxation time, five typical pore points of different scales were selected in the matching

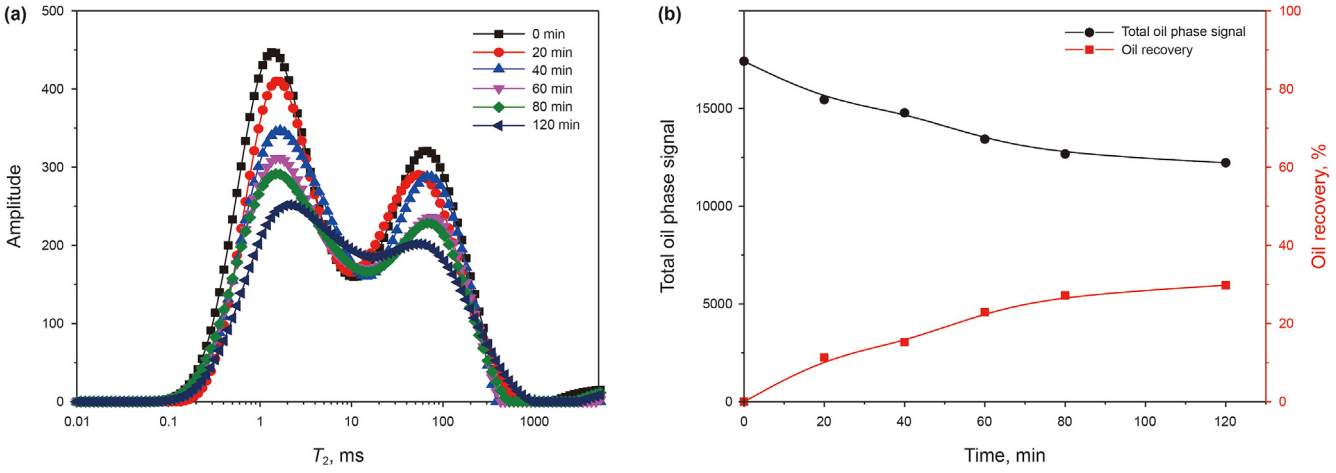

Fig. 4. (**a**) Typical T_2 spectra and (**b**) oil recovery during the dynamic imbibition process of the matrix-fracture core.

map of the T_2 spectrum and the mercury intrusion data, and the conversion coefficient was calculated, as reported in Table 3. The mean value of the calculation results at the representative points was used for the conversion coefficient, which was 0.558 μm/ms.

After the conversion factor was obtained, the amplitude-relaxation time curve of the T_2 spectra during the dynamic imbibition process was converted into the amplitude-pore diameter curve. Fig. 7 presents the amplitude–pore diameter curve obtained by the conversion factor for the typical dynamic imbibition process at the displacement flow rate of 0.1 mL/min.

Fig. 7 shows that during the dynamic imbibition process, the signal amplitudes of both the micropores and macropores were significantly reduced, indicating that the oil in the small and large pores was effectively discharged during the dynamic imbibition process. This is because the capillary force of the small pores was large, the wetting phase (water phase) tended to enter the small pores, and the oil in the small pores was displaced into the mesopores or macropores, thereby reducing the amount of oil in the small pores. Macropores are larger and have lower seepage resistance. Under the action of the displacement pressure during the dynamic imbibition, the oil phase could also be effectively discharged due to the lower seepage resistance. On the other hand, the capillary force and displacement pressure difference in the mesopores were not dominant, and it was difficult for water to enter the mesopores to displace the oil. The mesopores were mainly used as oil expulsion channels for micropores and macropores, and the change in the amount of oil in the mesopores was not obvious. This analysis reveals that during dynamic imbibition, the oil was mainly produced from the macropores and micropores, and the contribution of the mesopores to the total oil recovery was relatively low. In addition, there is a "lift" at the end of the curve, which is because the oil phase in the matrix entered the fracture after being discharged, which manifested as an oil phase signal in the fracture.

After obtaining the amplitude–pore size diagram of the dynamic imbibition process, the matrix pores were divided into different scale ranges according to the signal peaks: 0.01–1.00 μm is defined as micropores, 1.00–30.00 μm is defined as mesopores, and 30.00–400.00 μm is defined as macropores. Via the conversion coefficient C (0.558 μm/ms), the relaxation time range in the T_2 spectra corresponding to pores with different scale ranges was obtained (Table 4).

Via the changes in the oil phase signal amplitude within different pore scale ranges (or the corresponding T_2 spectral relaxation time ranges), the oil recovery changes in pores of different sizes during the dynamic imbibition were calculated using Eq. (2). The results are presented in Fig. 8.

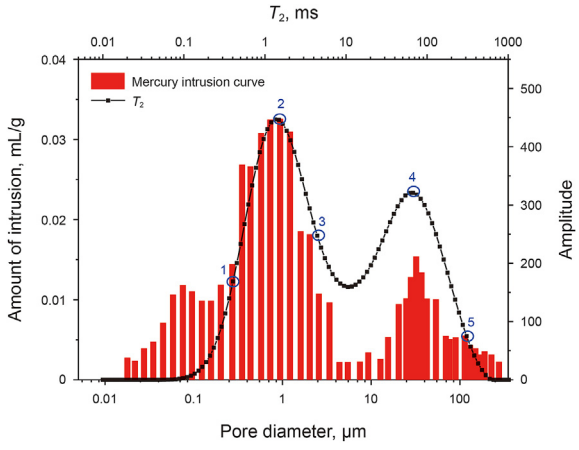

Fig. 6. The matching of the T_2 spectrum with the mercury intrusion data.

In the early stage of dynamic imbibition, the oil recovery factors of the micropores and macropores both increased significantly, while that of the mesopores remained basically unchanged. This was caused by the combined effect of the capillary force and displacement pressure during dynamic imbibition. The capillary force in the micropores was large, and the wetting phase (water phase) preferentially entered the micropores to displace the oil. For the macropores, due to the low seepage resistance, the water phase more easily entered the pores under the displacement pressure, and the oil in macropores was displaced. However, the mesopores, which were not dominant in the capillary force and the seepage capacity, were mainly used as the oil flow channels. The oil in the micropores and macropores was displaced in the fractures through the mesopores. In the initial stage, the amount of oil entering the mesopores was basically equal to the amount of oil expelled, resulting in the basically unchanged oil recovery of the mesopores. With the progression of the dynamic imbibition, the oil expulsion rate in the micropores and macropores decreased, while the oil in the mesopores was continuously discharged and carried by the fluid flow in the fractures. Therefore, the oil expulsion from the mesopores exceeded the oil entry amount, thereby resulting in an increase in the oil recovery of the mesopores. In addition, during the dynamic imbibition, the oil recovery in the mesopores and macropores decreased at a certain time, which may be because the oil phase in the small pores was displaced to the mesopores or macropores via imbibition. This increased the amount of oil in the mesopores or macropores at a certain stage, resulting in fluctuations in their oil recovery. Based on the final oil recovery results of pores with different scales, during the typical dynamic imbibition process at the optimal flow rate of 0.1 mL/min, the oil recovery of the micropores was the highest (50.4%), followed by that of the macropores (28.6%), and that of the mesopores was the lowest (15.8%).

3.4. Mechanism of the influence of the flow rate on the dynamic imbibition oil recovery

The oil recovery of different-sized pores during dynamic imbibition at different displacement flow rates was determined via the method discussed previously using a series of T_2 spectra measured at different flow rates. The final oil recovery for typical pore sizes (0.5, 2.0, 19.5, 51.9 μm) of dynamic imbibition at different flow rates are shown in Fig. 9.

It can be seen from Fig. 9 that with the decrease in the displacement rate, the oil recovery of the small pores (0.5 μm) increased obviously, while that of the large pores (51.9 μm) decreased obviously. For the mesoscale pores (2.0 and 19.5 μm), the oil recovery exhibited no significant change. These results indicate that the flow rate variation of dynamic imbibition mainly affected the oil expulsion characteristics of large and small pores. Additionally, the oil expulsion characteristics of the micropores and macropores were the key factors affecting the total oil recovery of the core sample during dynamic imbibition. Therefore, the subsequent discussion of the influence mechanism primarily focuses on the micropores and macropores.

Fig. 10 presents the effect of the flow rate on the oil recovery of the micropores (<1.0 μm), the oil recovery of the macropores (>30.0 μm), and the total oil recovery of the tight sandstone core.

With the decrease in the flow rate, the oil recovery of the micropores increased significantly, that of the macropores decreased significantly, and the total oil recovery exhibited an obvious increase followed by a slight decrease. The total oil recovery increased from 15.1% at the flow rate of 0.4 mL/min to the highest value of 29.8% at the flow rate of 0.1 mL/min. Thus, a high

Table 3
The calculation of the conversion factor.

Serial number	Relaxation time T_2, ms	Pore diameter d, μm	Conversion factor C, μm/ms
1	0.40	0.27	0.675
2	1.49	0.94	0.631
3	4.42	2.57	0.581
4	67.11	32.12	0.479
5	307.74	130.33	0.424
Average value			0.558

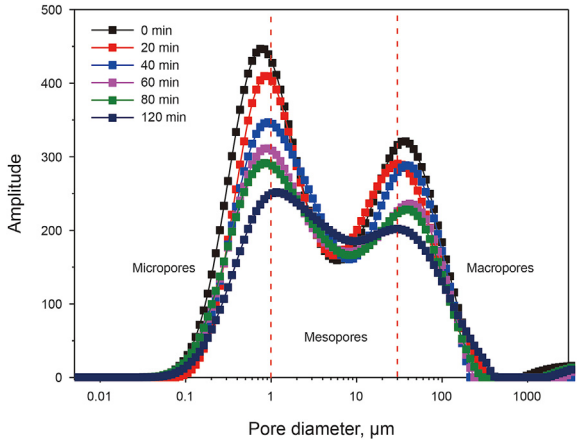

Fig. 7. The amplitude–pore size curve of dynamic imbibition at the flow rate of 0.1 mL/min.

Table 4
The pore size classification.

Pore type	Pore diameter, μm	Corresponding relaxation time, ms
Micropores	0.01–1.00	0.02–1.79
Mesopores	1.00–30.00	1.79–53.76
Macropores	30.00–400.00	53.76–716.85

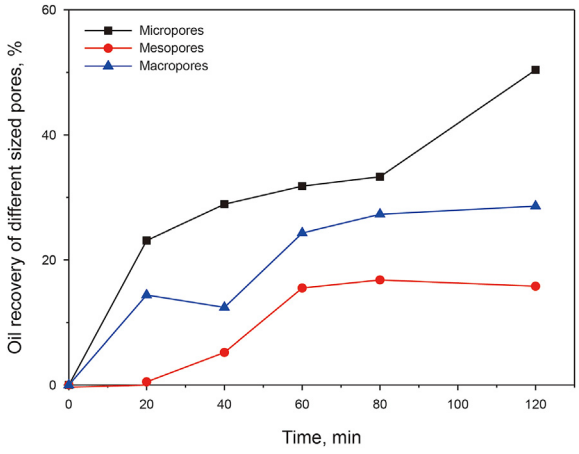

Fig. 8. The variation of the oil recovery with the dynamic imbibition time in pores of different sizes.

displacement flow rate could only increase the oil expulsion rate (the T_2 spectra quickly reached a stable state), and was not conducive to the improvement of the total oil recovery.

The capillary number reflects the relationship between the driving force and resistance in the two-phase displacement process. To quantitatively characterize and explore the oil expulsion

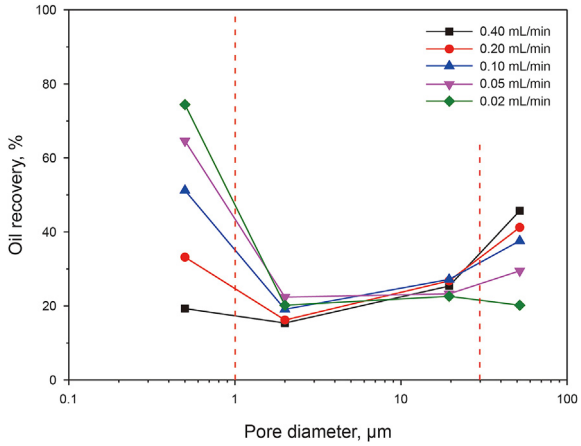

Fig. 9. The oil recovery for typical pore sizes of dynamic imbibition at different flow rates.

mechanisms of different pores during dynamic imbibition at different flow rates, the capillary numbers of the micropores and macropores were determined by Eq. (4).

$$N_c = \frac{\mu v}{\sigma}, \tag{4}$$

where N_c is the capillary number; μ is the displacement fluid viscosity, Pa s; σ is the oil–water interfacial tension, N/m; and v is the displacement rate in the pores, m/s. The displacement rate (v), which is equal to the oil expulsion rate in the pores, can be calculated by the volume method, as given by Eqs. (5)–(7).

$$R \times P_v = V_o = v \times t \times S, \tag{5}$$

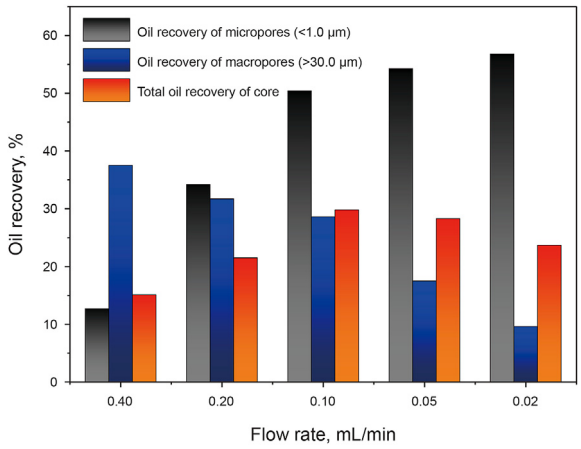

Fig. 10. The dynamic imbibition oil recovery at different displacement flow rates.

Table 5
The oil recovery, capillary number, and recovery ratio of dynamic imbibition at different flow rates.

Flow rate, mL/min	Micropores (<1.0 μm)		Macropores (>30.0 μm)		Recovery ratio	Total oil recovery, %
	Oil recovery, %	Capillary number, × 10^{-6}	Oil recovery, %	Capillary number, × 10^{-6}		
0.4	13.7	4.43	37.5	12.1	0.9	15.1
0.2	33.2	9.11	31.7	8.63	3.0	21.5
0.1	50.4	10.3	28.6	7.85	4.8	29.8
0.05	56.4	14.0	20.1	4.04	8.5	28.3
0.02	61.8	18.4	11.6	2.13	16.2	23.7

where R is the oil recovery, %; P_v is the pore volume, m^3; V_o is the volume of oil produced, m^3; t is the time with the amplitude change in the T_2 spectra, s; and S is the oil expulsion area of different pores on the fracture surface, m^2.

The calculation of the capillary number of micropores is taken as an example.

$$R_s \times V_{core} \times \phi \times \varphi_s = V_{os} = v_s \times t \times S_s, \tag{6}$$

$$S_s = 2 \times S_f \times \phi \times \varphi_s, \tag{7}$$

where R_s is the oil recovery of the micropores, %; V_{core} is the core volume, m^3; ϕ is the porosity of the core sample, %; and φ_s is the volume ratio of micropores to the total pores in the core, %, which can be obtained from mercury intrusion testing; additionally, V_{os} is the amount of oil expelled from the micropores, m^3; v_s is the displacement rate in the micropores, m/s; t is the time with the amplitude change in the T_2 spectra, s; S_s is the area of micropores on the fracture surface, m^2; and S_f is the area of the fracture surface, m^2.

Additionally, to quantitatively characterize the contribution of oil expulsion in different pores to the total oil recovery, the recovery ratio (γ) is defined and calculated by Eq. (8):

$$\gamma = \frac{R_s V_s}{R_b V_b} = \frac{R_s \varphi_s}{R_b \varphi_b}, \tag{8}$$

where γ is the recovery ratio of micropores to macropores; R_b is the oil recovery of the macropores, %; and φ_b is the volume ratio of the

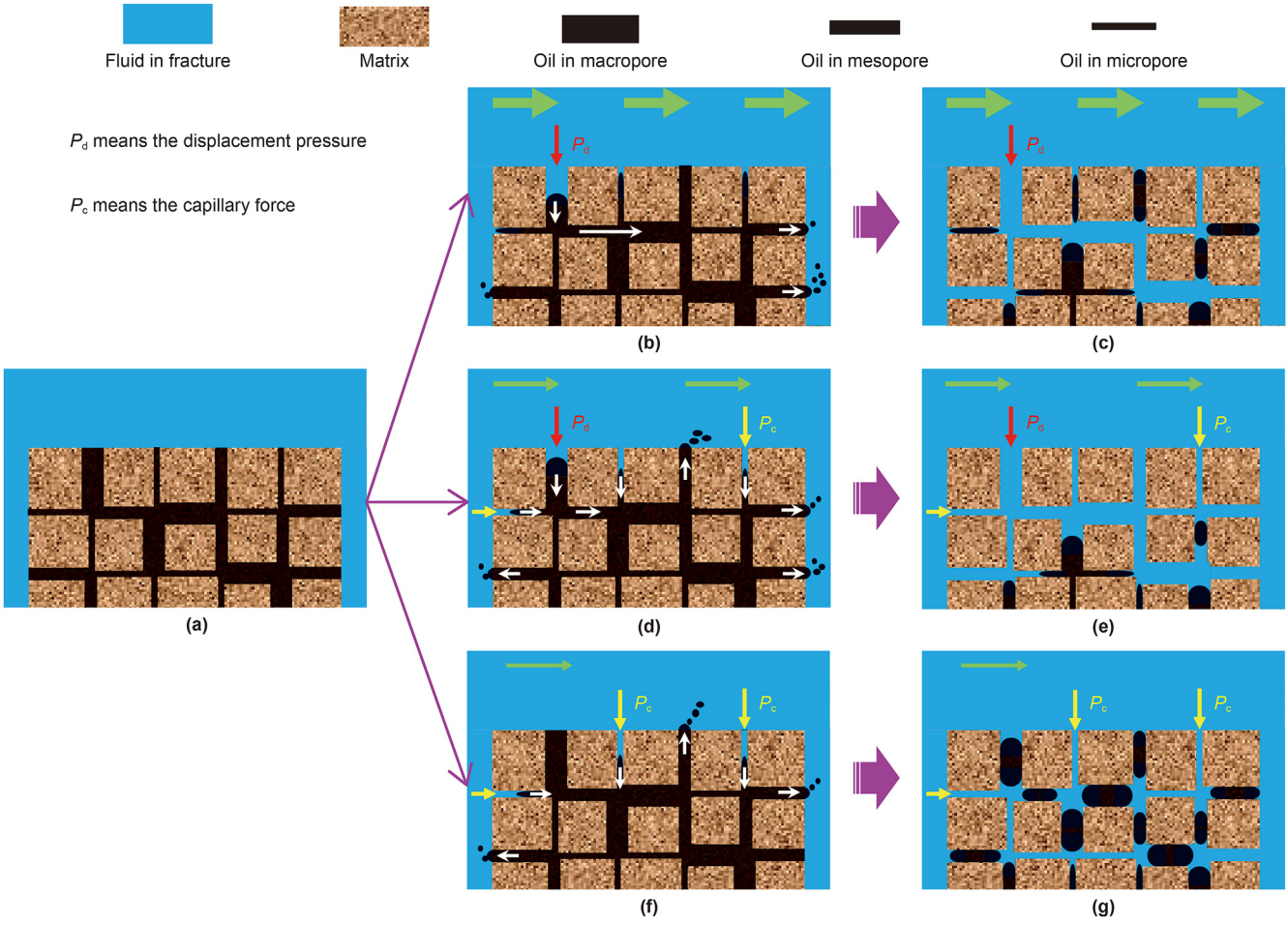

Fig. 11. The schematic diagram of the synergistic mechanism of the displacement pressure difference and the capillary force during the dynamic imbibition. (**a**) Initial state of the matrix-fracture flow unit; (**b**) Oil expulsion at a high flow rate; (**c**) Final state of dynamic imbibition at a high flow rate; (**d**) Oil expulsion at a moderate flow rate; (**e**) Final state of dynamic imbibition at a moderate flow rate; (**f**) Oil expulsion at a low flow rate; (**g**) Final state of dynamic imbibition at a low flow rate.

macropores to the total pores in the core, %. It follows from the mercury intrusion data that the volume ratio of micropores was about 52.0%, and the volume ratio of macropores was about 19.0%.

Table 5 reports the calculation results of the oil recovery and capillary numbers of the micropores and macropores, and the recovery ratios of the micropores to the macropores for dynamic imbibition at different flow rates.

The results in Table 5 indicate that as the flow rate decreased, the oil recovery and capillary number of the micropores increased, while those of the macropores decreased. With the decrease in the flow rate to 0.2 mL/min, the capillary number of the micropores began to exceed that of the macropores. Moreover, the recovery ratio of the micropores to the macropores increased obviously with the decrease in the flow rate. These results indicate that the oil expulsion efficiency and the contribution of the micropores to the total oil recovery significantly increased with the decrease in the flow rate. This is because the dynamic imbibition process occurred under the synergy of the capillary force and displacement force. When the flow rate decreased, the capillary number of the micropores increased, which means the dynamic imbibition was mainly driven by the capillary force in the micropores. When the flow rate increased, the capillary number of the macropores increased, which means the effect of the displacement pressure in the macropores played an increasingly important role in the dynamic imbibition process. This in turn increased the oil recovery of the macropores, and the recovery ratio of the micropores to the macropores decreased.

Based on the preceding discussion, the mechanism of the influence of the flow rate on the oil recovery of dynamic imbibition can be explained by the combined action of the capillary force and the displacement pressure during the dynamic imbibition process, as shown in Fig. 11. At a high flow rate, the oil in the macropores was effectively expelled driven by displacement pressure (P_d). Moreover, due to the connectivity and seepage in the porous media, the oil expulsion driven by the capillary force (P_c) in the micropores was inhibited. At this time, large amounts of remaining oil were trapped in the micropores and the mesopores, as shown in Fig. 11b and c. This indicates that the capillary number and oil recovery of the macropores were higher than those of the micropores and the mesopores at a high flow rate, as reported in Table 5. Similarly, when the flow rate was low, the oil expulsion driven by P_c in the micropores was obvious, and the effect of P_d was weak. At this time, large amounts of remaining oil were trapped in the macropores and the mesopores, as shown in Fig. 11f and g. Because the volume proportion of the micropores was the highest (52.0%) for the cores used in this study, the total oil recovery of dynamic imbibition at a low flow rate was higher than that at a high flow rate. However, due to the difficulty of oil expulsion in the macropores and the mesopores, the total oil recovery remained unable to achieve the optimal value. Only at a moderate flow rate did P_c and P_d both have significant effects on oil expulsion, and the oil in different sized pores was effectively expelled, as shown in Fig. 11d and e. This resulted in the highest ultimate total oil recovery of dynamic imbibition.

4. Conclusions

(1) With the increase in the displacement flow rate, the oil recovery of dynamic imbibition has a maximum value at a specific flow rate. In this study, the optimal flow rate for dynamic imbibition was 0.1 mL/min, and the oil recovery increased from 23.2% during static imbibition to 29.8% during dynamic imbibition at the optimal flow rate.

(2) During dynamic imbibition at the optimal displacement rate (0.1 mL/min), the oil recovery of the micropores (0.01–1.00 μm in diameter) was the highest (50.4%), followed by that of the macropores (30.00–400.00 μm in diameter) of 28.6%, and that of the mesopores (1.00–30.00 μm in diameter) was the lowest (15.8%).

(3) The oil expulsion efficiency and the contribution to total oil recovery of the micropores were found to significantly increase with the decrease in the flow rate, while the opposite was true for the macropores.

(4) During dynamic imbibition at a low flow rate, the oil in the micropores was effectively expelled driven by capillary force, and the effect of displacement pressure was weak, leading to large amounts of remaining oil trapped in the macropores. On the contrary, when the flow rate was too high, large amounts of remaining oil would be trapped in the micropores. Only at a moderate flow rate did the capillary force and displacement pressure both have significant effects on oil expulsion, and the oil in different sized pores was effectively expelled, thus generating a relatively high total oil recovery.

Acknowledgments

This work was supported by the National Natural Science Foundation of China (Grant No. 52104061), the National Key Research and Development Project (Grant No. 2019YFA0708700), the project funded by the China Postdoctoral Science Foundation (Grant No. 2020M682264), the Shandong Provincial Natural Science Foundation (Grant No. ZR2021QE075) and the Fundamental Research Funds for the Central Universities (Grant No. 20CX06090A).

References

Adibhatla, B., Mohanty, K.K., 2008. Parametric analysis of surfactant-aided imbibition in fractured carbonates. J. Colloid Interface Sci. 317 (2), 513–522. https://doi.org/10.1016/j.jcis.2007.09.088.

Al-Attar, H.H., 2010. Experimental study of spontaneous capillary imbibition in selected carbonate core samples. J. Petrol. Sci. Eng. 70 (3–4), 320–326. https://doi.org/10.1016/j.petrol.2009.12.003.

Babadagli, T., 2002. Dynamics of capillary imbibition when surfactant, polymer, and hot water are used as aqueous phase for oil recovery. J. Colloid Interface Sci. 246 (1), 203–213. https://doi.org/10.1006/jcis.2001.8015.

Cheng, Z., Wang, Q., Ning, Z., et al., 2018. Experimental investigation of counter-current spontaneous imbibition in tight sandstone using nuclear magnetic resonance. Energy Fuel. 32 (6), 6507–6517. https://doi.org/10.1021/acs.energyfuels.8b00394.

Cheng, Z., Ning, Z., Yu, X., et al., 2019. New insights into spontaneous imbibition in tight oil sandstones with NMR. J. Petrol. Sci. Eng. 179, 455–464. https://doi.org/10.1016/j.petrol.2019.04.084.

Civan, F., Rasmussen, M.L., 2003. Modeling and validation of hindered-matrix-fracture transfer for naturally fractured petroleum reservoirs. In: SPE Production and Operations Symposium. https://doi.org/10.2118/80918-MS.

Civan, F., Rasmussen, M.L., 2005. Determination of parameters for matrix-fracture transfer functions from laboratory data. In: SPE Production Operations Symposium. https://doi.org/10.2118/94267-MS.

Dai, C., Cheng, R., Sun, X., et al., 2019. Oil migration in nanometer to micrometer sized pores of tight oil sandstone during dynamic surfactant imbibition with online NMR. Fuel 245, 544–553. https://doi.org/10.1016/j.fuel.2019.01.021.

Dou, L., Xiao, Y., Gao, H., et al., 2021. The study of enhanced displacement efficiency in tight sandstone from the combination of spontaneous and dynamic imbibition. J. Petrol. Sci. Eng. 199, 108327. https://doi.org/10.1016/j.petrol.2020.108327.

Fallah Fini, M., Riahi, S., Bahramian, A., 2012. Experimental and QSPR studies on the effect of ionic surfactants on *n*-decane-water interfacial tension. J. Surfactants Deterg. 15, 477–484. https://doi.org/10.1007/s11743-012-1330-7.

Hatiboglu, C.U., Babadagli, T., 2007. Oil recovery by counter-current spontaneous imbibition: effects of matrix shape factor, gravity, IFT, oil viscosity, wettability, and rock type. J. Petrol. Sci. Eng. 59 (1–2), 106–122. https://doi.org/10.1016/j.petrol.2007.03.005.

Jiang, Y., Shi, Y., Xu, G., et al., 2018. Experimental study on spontaneous imbibition under confining pressure in tight sandstone cores based on low-field nuclear magnetic resonance measurements. Energy Fuel. 32 (3), 3152–3162. https://doi.org/10.1021/acs.energyfuels.7b03776.

Kathel, P., Mohanty, K.K., 2013. Wettability alteration in a tight oil reservoir. Energy Fuel. 27 (11), 6460–6468. https://doi.org/10.1021/ef4012752.

Li, D., Liu, Z., Zhang, G., et al., 2017. Comparison and revelation of tight oil

accumulation conditions, distribution characteristics and development status between China and US. Nat. Gas Geosci. 28 (7), 1126–1138. https://doi.org/10.11764/ji.ssn.1672G1926.2017.07.004.
Liu, J., Sheng, J.J., 2020. Investigation of countercurrent imbibition in oil-wet tight cores using NMR technology. SPE J. 25, 2601–2614. https://doi.org/10.2118/201099-PA.
Liu, Y.F., Zou, C.W., Zhou, D.Y., et al., 2019. Novel chemical flooding system based on dispersed particle gel coupling in-depth profile control and high efficient oil displacement. Energy Fuel. 33 (4), 3123–3132. https://doi.org/10.1021/acs.energyfuels.9b00243.
Lowden, B.D., Porter, M.J., Powrie, L.S., 1998. T_2 relaxation time versus mercury injection capillary pressure: implications for NMR logging and reservoir characterisation. In: European Petroleum Conference. https://doi.org/10.2118/50607-MS.
Meng, Q., Liu, H., Wang, J., et al., 2016. Effect of gravity on spontaneous imbibition from cores with two ends open in the frontal flow period. J. Petrol. Sci. Eng. 141, 16–23. https://doi.org/10.1016/j.petrol.2016.01.024.
Meng, Z., Yang, S.L., Cui, Y., et al., 2018. Enhancement of the imbibition recovery by surfactants in tight oil reservoirs. Petrol. Sci. 15, 783–793. https://doi.org/10.1007/s12182-018-0253-y.
Morrow, N.R., Mason, G., 2001. Recovery of oil by spontaneous imbibition. Curr. Opin. Colloid Interface 6 (4), 321–337. https://doi.org/10.1016/S1359-0294(01)00100-5.
Sharma, G., Mohanty, K.K., 2013. Wettability alteration in high-temperature and high-salinity carbonate reservoirs. SPE J. 18, 646–655. https://doi.org/10.2118/147306-PA.
Sun, L., Zou, C., Jia, A., et al., 2019. Development characteristics and orientation of tight oil and gas in China. Petrol. Explor. Dev. 46 (6), 1073–1087. https://doi.org/10.1016/S1876-3804(19)60264-8.
Sun, Y., Gao, K., Yu, Z., et al., 2020. Dynamic imbibition with aid of surfactant in tight oil fracture network model. J. Petrol. Sci. Eng. 193, 107393. https://doi.org/10.1016/j.petrol.2020.107393.
Tangirala, S., Sheng, J.J., 2019. Roles of surfactants during soaking and post leak-off production stages of hydraulic fracturing operation in tight oil-wet rocks. Energy Fuel. 33 (9), 8363–8373. https://doi.org/10.1021/acs.energyfuels.9b01913.
Tavassoli, Z., Zimmerman, R.W., Blunt, M.J., 2005. Analysis of counter-current imbibition with gravity in weakly water-wet systems. J. Petrol. Sci. Eng. 48 (1–2), 94–104. https://doi.org/10.1016/j.petrol.2005.04.003.
Umeobi, H.I., Li, Q., Xu, L., et al., 2021. NMR Investigation of brine imbibition dynamics in pores of tight sandstones under different boundary conditions. Energy Fuel. 35 (19), 15856–15866. https://doi.org/10.1021/acs.energyfuels.1c01417.
Wang, J., Liu, H., Xia, J., et al., 2017. Mechanism simulation of oil displacement by imbibition in fractured reservoirs. Petrol. Explor. Dev. 44 (5), 805–814. https://doi.org/10.1016/S1876-3804(17)30091-5.
Wang, J., Liu, H., Qian, G., et al., 2019. Investigations on spontaneous imbibition and the influencing factors in tight oil reservoirs. Fuel 236, 755–768. https://doi.org/10.1016/j.fuel.2018.09.053.
Wang, X., Peng, X., Zhang, S., et al., 2018. Characteristics of oil distributions in forced and spontaneous imbibition of tight oil reservoir. Fuel 224, 280–288. https://doi.org/10.1016/j.fuel.2018.03.104.
Yang, L., Ge, H., Shi, X., et al., 2016. The effect of microstructure and rock mineralogy on water imbibition characteristics in tight reservoirs. J. Nat. Gas Sci. Eng. 34, 1461–1471. https://doi.org/10.1016/j.jngse.2016.01.002.
Yang, Z., Liu, X., Li, H., et al., 2019. Analysis on the influencing factors of imbibition and the effect evaluation of imbibition in tight reservoirs. Petrol. Explor. Dev. 46 (4), 779–785. https://doi.org/10.1016/S1876-3804(19)60235-1.
Yildiz, H.O., Gokmen, M., Cesur, Y., 2006. Effect of shape factor, characteristic length, and boundary conditions on spontaneous imbibition. J. Petrol. Sci. Eng. 53 (3–4), 158–170. https://doi.org/10.1016/j.petrol.2006.06.002.
You, Q., Wang, H., Zhang, Y., et al., 2018. Experimental study on spontaneous imbibition of recycled fracturing flow-back fluid to enhance oil recovery in low permeability sandstone reservoirs. J. Petrol. Sci. Eng. 166, 375–380. https://doi.org/10.1016/j.petrol.2018.03.058.
Zhu, W.Y., Yue, M., Liu, Y.F., et al., 2019. Research progress on tight oil exploration in China. Chin. J. Eng. 41 (9), 1103. https://doi.org/10.13374/j.issn2095-9389.2019.09.001.
Zou, C., Yang, Z., Tao, S., et al., 2012. Nano-hydrocarbon and the accumulation in coexisting source and reservoir. Petrol. Explor. Dev. 39 (1), 15–32. https://doi.org/10.1016/S1876-3804(12)60011-1.
Zou, C.N., Zhu, R.K., Bai, B., et al., 2015. Significance, geologic characteristics, resource potential and future challenges of tight oil and shale oil. Bull. China Soc. Mineral Petrol. Geochem. 34 (1), 3–17. https://doi.org/10.3969/j.issn.1007-2802.2015.01.001.